STEPWISE DEVELOPMENT TESTING AND TECHNOLOGY DEMONSTRATION OF A LANDING SYSTEM WITH LANDING LEGS

R. Buchwald[1] , M. Klaus[2] , J. Bolz[1], A. Dafnis[2] , H.-G. Reimerdes[2]

[1] Astrium GmbH, Airbusallee 1, 28199 Bremen, Email: robert.buchwald@astrium.eads.net

[2] Lehrstuhl und Institut für Leichtbau, RWTH Aachen, Wüllnerstraße 7, 52062 Aachen,
Email: info@ilb.rwth-aachen.de

Abstract

One of the major milestones during the development of a landing system for robotic or manned exploration is the analyses and verification of the chosen design on Earth. Prerequisite for a successful verification is a realistic representation of the touchdown conditions and the target landing site properties in a laboratory environment. In particular the lower gravitational acceleration as it is present on Moon, Mars, comets or asteroids is a key driver for the design of the landing subsystem with respect to landing stability issues. Due to the fact that usually not all relevant environmental properties of the target landing site can be provided in one single and complete test, any verification approach has to be strongly supported by adequate numerical analyses.

In 2008, a generic research study has been set up by the Astrium GmbH, funded by R&D money[1] and coordinated with the current European mission studies. The main purposes of these research activities are the successive increase of the technological maturity and knowledge of the landing subsystem up to TRL 5-6 and the development, correlation and validation of the dedicated numerical software tools.

Within the used stepwise test and verification approach the complexity and level of integration is successively increased on breadboard and numerical analyses side in parallel. On each level of integration the numerical models are correlated with the results of the development tests. The paper will give a look inside of the performed tests and the achieved results. Special focus will be set on the discussion of the representativeness of the chosen test scenarios and numerical tools and the applicability for future mission studies.

1. LANDER DESIGN CONCEPTS

1.1. Lander System Design

In the past various types of landing systems with landing legs have been used. Successful lunar missions with landing legs were NASA's Surveyor and Apollo and the Russian Luna programme. Successful Mars missions with landing legs were NASA's Viking missions and the NASA Phoenix mission.

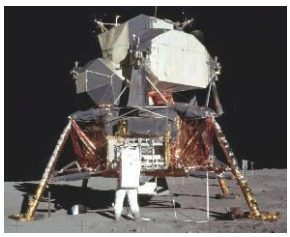

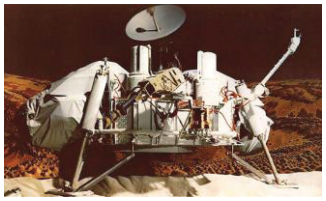

Fig. 1: left: *Apollo Lunar Module,* right: *Viking Lander* (Credit: NASA)

In all successful designs, the landing gear systems were consisting of three or four legs with integrated shock absorbing elements which were designed for surviving one touchdown. The system has to limit the loads on the platform, provide static and dynamic stability against toppling at any time of the mission and has to be as lightweight and compact as possible to minimise the system mass and stowing space.

1.2. Landing Leg Design

Basically two types of landing legs can be distinguished. Both of them consist of a primary strut, which contains the main shock absorber, and two secondary struts or an A-Frame structure for the lateral support of the main damper.

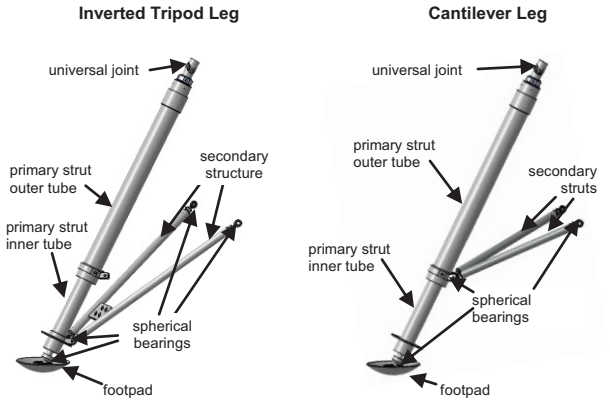

Fig. 2: Landing leg configurations

All Lunar missions after Surveyor used the so called *Cantilever Leg*. In this configuration, the secondary struts are connected via ball joints to the outer tube of the main shock absorber. The inner tube is connected to the footpad and guided by bearings within the outer tube. The lateral loads acting on the primary shock absorber induced by the secondary struts are limited by damping elements inside or attached to the secondary struts.

[1] Since autumn 2010 the activities are co-funded by the DLR within the German national Triple-A study (Förderkennzeichen 50RA1030)

In the *Inverted Tripod* configuration, the secondary support structure is connected to the footpad (Viking type) or to the inner tube of the primary strut damper. This leads to almost negligible bending loads on the primary absorber but to a significant loss of ground clearance due to the kinematical properties of the legs when the primary damper is deformed.

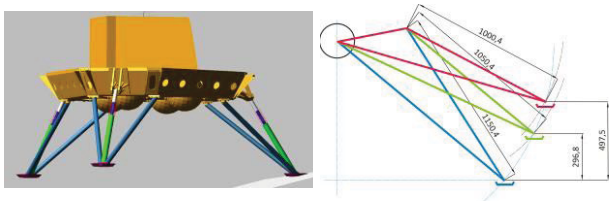

Fig. 3: Ground clearance loss due to damper stroke

The Inverted Tripod configuration has been used for all Mars missions so far. For Mars missions, no large propulsion elements are situated under the platform. Furthermore, the complete system is designed highly compact to fit into the heat shield.

Under these circumstances and in a landing region with moderate slopes and rock sizes (e.g. below 15° of local slopes and 200-300mm rock height), the Inverted Tripod design usually leads to a lower system mass than the Cantilever leg type even if the leg deployment mechanism is in most cases more complex. For a lunar missions or landing sites with a high number of large rocks, the Cantilever Leg can be significantly lighter.

1.3. Shock Absorber Design

Independent from the leg type, the main shock absorber incorporated in almost all designs are plastically deformable aluminium honeycomb cylinders for the absorption of the kinetic energy at touchdown and the limitation of the structure borne loads on the platform. The force-stroke characteristics of the dedicated absorbers have been adjusted to the specific needs of each mission by staggering honeycombs of different densities.

In contrast to the primary strut shock absorbers, which are never loaded under tension, the secondary struts have to limit the occurring loads under compression and tension. Since the capability of Aluminium honeycomb material to dissipate energy under tension is highly limited, complex honeycomb cartridge designs are necessary to transform tensile strut loads into compression loads for the honeycombs for these load cases. This design concept has for example been used for the Apollo Lunar Module.

All Mars mission designs of the NASA were using bending pins (often just called *Load Limiters*) between the secondary struts and the platform instead of the more complex honeycomb cartridges for the limitation of lateral shocks on the system. Load Limiters are simple metallic rods, which are loaded laterally by the axial force of a secondary strut and deform under tension and compression without any additional mechanism. Although the simplicity of this solution is very attractive, the force / stroke characteristic of these rods is only adjustable within narrow ranges by the choice of the rod material, diameter and length and the angle between the rod and the secondary struts. For this reason, this solution is only applied for smaller landing probe concepts up to a touch down mass of about 1 to.

2. REQUIREMENTS AND VERIFICATION

2.1. Future Mission Scenarios

Beside currently ongoing activities to explore other celestial bodies of our solar system (asteroids, comets, Mercury or the Mars moon Phobos) the robotic exploration of Mars and Moon is still in the focus of almost all space agencies worldwide.

One of the next missions where particularly landing legs are planned to be used is the *European Lunar Lander*. The Lunar Lander Phase B1 is currently running under ESA lead with Astrium GmbH as the German prime contractor. The main objectives are to demonstrate a *soft and precision landing* at the south pole of the Moon with the capability to autonomously detect and avoid possible hazardous surface areas (e.g. large rocks, craters, local shadows) in the target landing zone (*Hazard Detection and Avoidance*) by using European technologies. In addition to the demonstration of these key functionalities, the objective is to deliver a scientific payload including a small rover to the lunar surface.

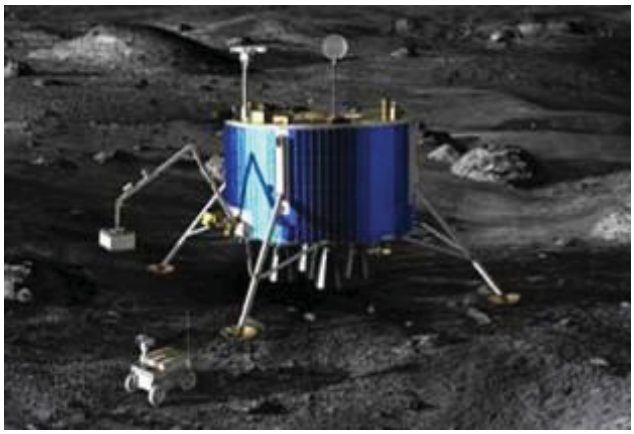

Fig. 4: Artist view of the ESA Lunar Lander

The demonstration of these capabilities is required as a preparation for a successful European contribution to the further robotic or human exploration of Moon and Mars or the first successful Mars sample return mission. A possible sample return scenario with the Sample Fetch Rover as European contribution is depicted in Fig. 5.

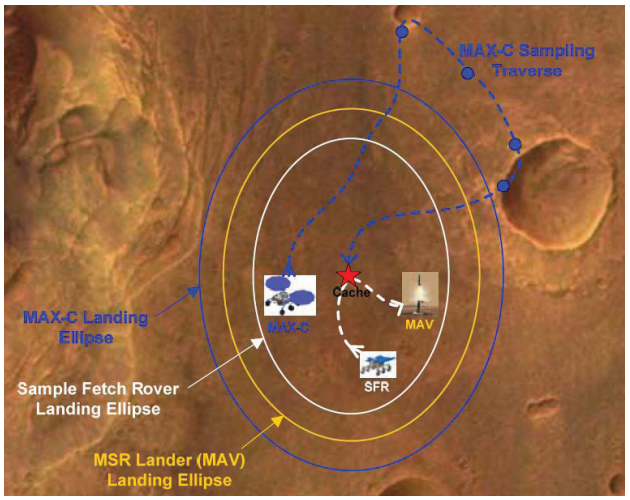

Fig. 5: Sample return scenario of the ESA Mars Precision Lander study (Source: ESA)

2.2. Landing System Requirements

The main functional requirements of the landing gear system are:

- to provide static and dynamic stability of the platform at any time during and after touchdown (3σ - probability of success)
- to limit the loads on the platform and the payload
- to be compliant with the available stowing space
- to avoid uncontrolled ground contact by any part of the lander except the footpads

The landing system design is driven by the need of finding a compromise between these system requirements which are partly in contradiction. As example, the induced platform acceleration can only be reduced by limitation of the forces in the damping elements. This leads to large deformations of the shock absorbers during touchdown and, as the logical consequence, to a larger landing gear in order to provide sufficient ground clearance (distance from the platforms lowest point to the ground) during touchdown. This might cause a conflict with the available stowing space.

Although in today's mission scenarios an uncontrolled contact of any part of the main structure with the ground is not desired most landing systems in the past were designed to survive at least a ground contact of the main nozzles.

2.3. Major Design Parameter

When defining a realistic test environment, the main influencing parameters for the landing system design and the performance verification of the landing legs need to be identified and transferred into representative test cases. On system level, these parameters can be divided up into three groups:

1. Landing site properties
    a. Compaction, flexibility and friction of the surface soil
    b. Local surface slopes and craters
    c. Size and distribution of rocks and boulders
    d. Gravitational acceleration
    e. Environmental temperature and atmospheric density

    Other conditions of the landing site like ground illumination or direct communication possibilities limit the possible target landing sites significantly and are therefore of course of interest for the *Hazard Detection and Avoidance* strategies. For the landing system, these effects are already covered by the definition of the above mentioned landing site properties.

2. Touchdown conditions
    a. Horizontal and Vertical touchdown velocities
    b. Platform attitude and attitude angular rate at touchdown
    c. Temperature of critical elements due to radiated heat from the nozzles, the heat shield (for Mars missions) and plume impingement due to reflections from the ground
    d. Amount and conditions of residual propellant at touchdown
3. Lander design parameter
    a. Platform mass and mass moments of inertia
    b. Position of the centre of mass of the platform
    c. Number and type of legs
    d. Platform interface
    e. Available stowing space

Due to the comparably challenging requirements for the European Lunar Lander and the Mars Sample Return scenarios, a clear design preference for the leg type or the number of legs cannot be stated a priori. For this reason both designs have been investigated in detail within this technology study in order to support the later system analyses.

2.4. Technology Breadboard Definition

Based on the functional and performance requirements on system level and on the identification of the major design elements, the requirements for each critical element of the following bottom - up verification process for the breadboard and the major functional properties of the landing leg demonstrator can be defined.

1. Main energy absorber

    The main energy absorber consists of three staggered Aluminium honeycombs incorporated in the main tube. In order to be representative for a variety of possible mission scenarios, generic crash level have been chosen with steps at 3.5, 7 and 11kN. The strain rate is assumed to be in the range of up to 4.5m/s in the direction of the strut.

2. Secondary Strut Load Limiter

    Due to the rather small landed mass within the Lunar Lander and the Mars Precision Lander scenario, it is assumed that a solution with bending rods is possible. For this reason, this solution is chosen for further investigation with a limitation level of about 3kN as baseline.

3. Geometric sizing

    The geometric dimensions are chosen to be in the range of a full scale demonstrator for a Mars mission and a scaled mock-up (50% of original size) with respect to the European Lunar Lander

4. Environmental conditions

    Due to the long firing duration at a powered descent on the Moon and due to the heat generated during an atmospheric entry on Mars a temperature clearly above standard room temperature is expected. Furthermore, when touching ground, the honeycombs will be completely evacuated. An influence of the low atmospheric density is not expected. This has to be respected in a representative test scenario.

2.5. Verification and Demonstration Approach

The verification and technology demonstration process starts bottom-up at the lowest level of integration. The level of representativeness successively increases with increasing level of integration up to a complete leg breadboard. A maximum number of tests have been performed on a low level of integration in order to minimise the costs and risks for the further development. In some cases, as e.g. for the Secondary Strut Load Limiter, the definition of a representative test environment was only possible on a higher level of integration. Therefore these tests were performed on assembly level.

In Fig. 6, an example for a complete development logic up to TRL 7 (Technology Readiness Level) is depicted. The performed demonstrations within this study cover most of the aspects up to TRL 6. Only the leg deployment and latching mechanisms and the footpad sensors are excluded.

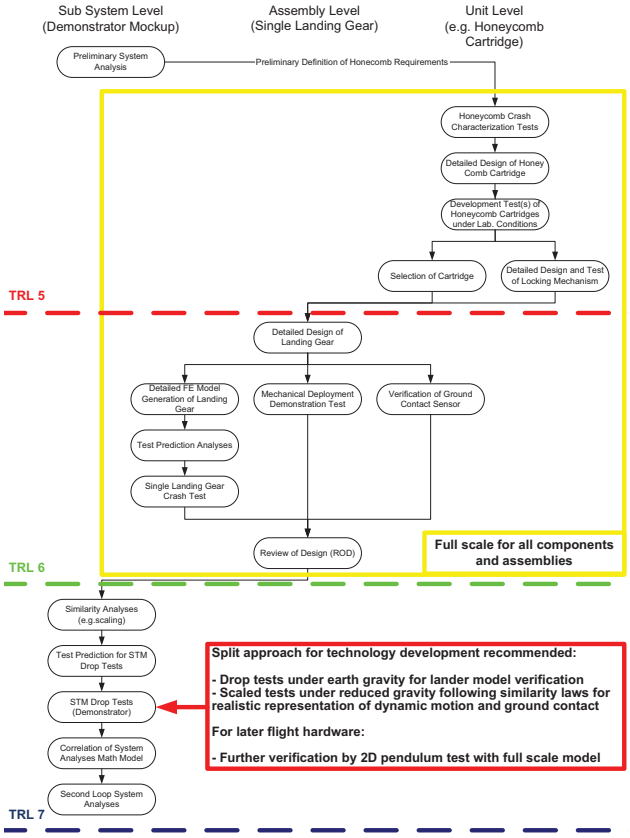

Fig. 6: Development logic up to TRL 7

3. TEST SETUPS, EXECUTION AND RESULTS

All in this paper presented tests were performed at the Chair and Institute of Aerospace and Lightweight Structures (Lehrstuhl und Institut für Leichtbau) of the RWTH Aachen University.

3.1. Material Characterisation Test

Following the bottom-up approach during the test program first the honeycomb shock absorbers alone were tested. To verify the properties of the honeycombs three tests series were performed:

- quasi-static compression tests at 25mm/min
- dynamic compression tests with a constant velocity at 2 m/s and 4 m/s
- dynamic compression tests with a drop tower with specimen temperatures of 20°-140° C

In all cases essentially the same test setup is used. The cube-shaped samples are compressed between a pair of parallel plates (see Fig. 7 and Fig. 8). During the dynamic tests the lower compression plate has a variety of counter-sank drill holes arranged in a grid. Additionally the sample and the plate are separated by a screen with 1mm holes in it. This arrangement allows the air to escape from the samples during the tests. The air trapped inside the honeycomb cells would otherwise affect the dynamic compression properties.

Fig. 7: Samples (*left*), lower compressing plate with air vents (*middle*) and upper compressing plate with a force sensor (*right*)

Fig. 8: Sample in the test set-up

The static tests were performed with a Schenk Hydropuls 160kN universal testing machine. During these tests the samples are compressed up to 3% of the length, unloaded and then compressed until the honeycomb walls are completely folded. An example of the according force-displacement-diagram is given in Fig. 9. The initial peak in force represents the initial critical load needed to create the first row of folds in the honeycomb walls. After this material triggering, the force-displacement curves follow a

saw tooth like path with small amplitude and a large constant offset. Every period of the saw teeth represents a new fold. If ignoring the initial peak the mean force remains virtually constant during the compression making the chosen material a reliable shock absorber.

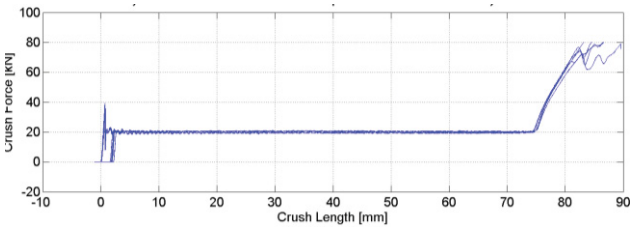

Fig. 9: Crush length vs. crush load, static compression

To reduce the impact shock during the dynamic tests the honeycomb samples are “pre-crashed” (meaning the first row is created statically prior to the actual test).

To characterize the dynamic properties of the honeycomb-samples the tests were repeated under dynamic conditions using a high strain rate machine (Instron VHS 65/25) to ensure crashing with a constant velocity (2 m/s and 4 m/s) (see Fig. 10).

Fig. 10: Instron VHS 65/25 high strain rate testing machine with the test set-up

The results are similar to the ones acquired during the static tests with a saw tooth like force-displacement curve around a mean force level. Using these tests and in comparison to the static compression tests a linear relation between the crush strength and the crush velocity seems to be applicable. The increase in crush strength due to the higher strain rate is about 10% at a crushing velocity of 4 m/s for the tested example given Fig. 11.

Finally the honeycomb samples are tested using a drop tower (see Fig. 12). During these tests a mass falls along a leading column and crashes on the sample which is placed on the perforated bottom plate. The kinetic energy of the drop mass with initial velocities of up to 4m/s is completely consumed by sample (or stacked samples) representing more realistic test conditions regarding the intended application as crash absorber.

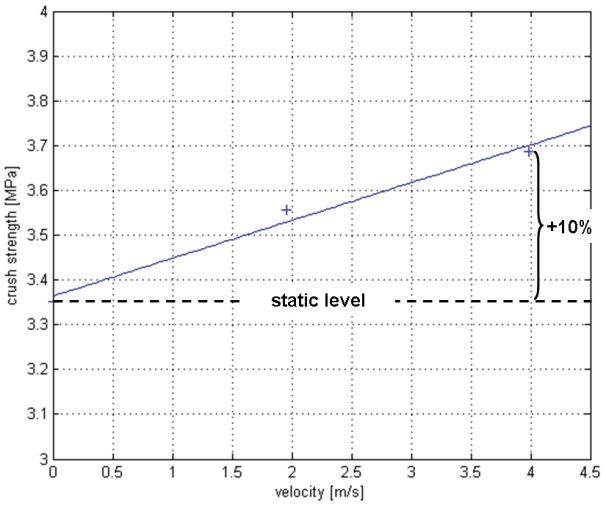

Fig. 11: Strain rate effect on honeycomb compression

The described drop tower tests were repeated with pre-heated samples to assess the temperature sensitivity of the compression behavior. Compression at room temperature, approx. 80°C and approx. 140°C were compared. The measured acceleration of the drop mass during the crushing is shown for these three temperatures in Fig. 13. The reduction in crush strength is significant (about 1/3 at 140°C).

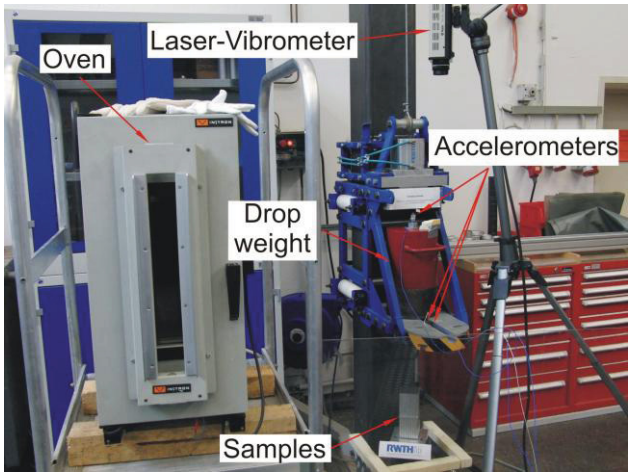

Fig. 12: Drop tower test set-up

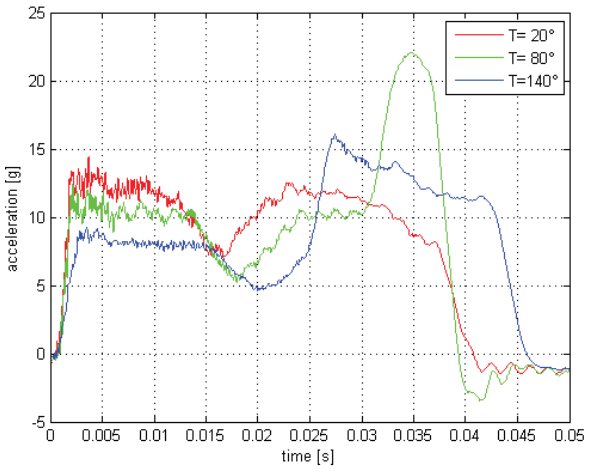

Fig. 13: Temperature influence on honeycomb compression

3.2. Secondary Strut Assembly

The secondary struts of a landing leg are connected to the lander by means of bending rods. The function of these rods is to limit lateral loads to the leg. The bending rods deforms plastically in the process. To investigate the behavior of the pins a test set-up is designed which mirrors the angles and the overall assembly in a possible leg configuration.

One side of the bending rod is clamped to the lower part of the setup at 40° to the horizontal. The other side is connected with a spherical joint to the secondary strut. The secondary strut is connected to the upper side of the test setup in a way which prevents the transfer of moments. The connection point of between the strut and the upper part of the setup is exactly above the clamping point of the bending rod to the lower part of the setup (see Fig. 14). The tests are performed using an INSTRON 600kN testing machine. The machine pushes the upper part of the setup down and after a certain deformation pulls it up again – changing constantly the angle between the strut and the rod and with it the orientation and length of the force vector applied to the bending rod. This is an approximation of a possible deformation cycle during landing.

Fig. 14: Secondary strut test set-up

The forces and displacements are measured by the testing machine. A set of complete cycles of 5 identical specimens is shown in Fig. 15. The cycles begin at the 0/0-position. The rods deform elastically at first and skip subsequently into plastic deformation. After loading direction is reversed (upper-right corner of the curve) the rod is again deformed first elastically and then plastically in the opposed direction, limiting the load for a very large stroke. If the load direction is reversed before the rod breaks after extensive material hardening (low-left corner of the curve) the cycle can be closed.

3.3. Primary Strut Assembly

Two tests series with the primary strut alone are performed – one for the final verification of the assembled primary damper and one for the characterization of the bearing friction inside of the primary strut.

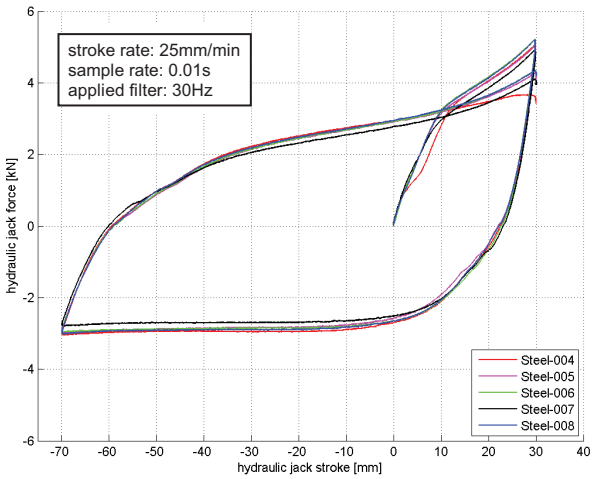

Fig. 15: Reproducibility of Load Limiter performance

3.3.1. Bearing Friction Characterisation

Especially if the cantilever leg configuration is used, lateral loads applied to the primary strut could change the performance characteristics significantly due to the internal bearing friction. Therefore, the increasing friction force between the linear bearings and the main tube of the primary strut due to lateral forces is investigated in these tests.

The primary strut is attached with a joint to a rigid plate at the bottom of the test setup and is fixed at the connection ring to the secondary struts. A constant lateral force is applied to the inner tube of the primary strut. The inner tube is them pushed into the main tube, measuring the force needed to do so. Also the force transferred through the sliding rings to the main tube is measured at the ending cap of the leg (see Fig. 16).

The relative displacement of the inner strut and the main tube are measured with a laser extensometer. The applied force increases up to a critical load F_{stat} and then the inner tube starts to slide into the outer tube keeping a almost constant load F_{dyn}. (See Fig. 17 for the exemplary force-time diagram). At 20 s into the test the movement of the inner strut is stopped leaving a residual force of approx. 50 N on the force sensors.

Fig. 16: Setup for bearing friction tests

The leg contains no honeycomb absorbers during these tests so all loads are transferred by means of friction. The tests were performed with lateral loads from 500N to 5kN.

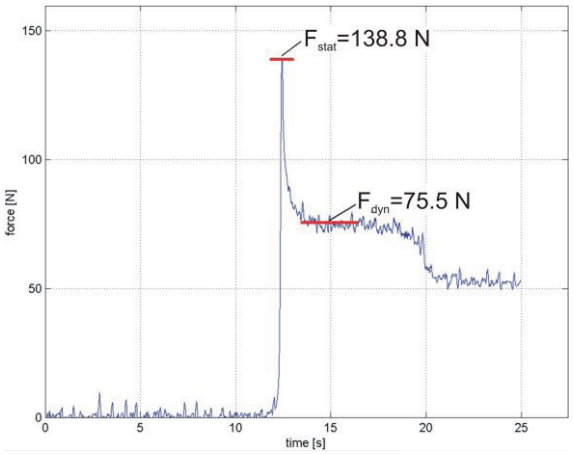

Fig. 17: Typical force history of the bearing friction tests

3.3.2. Primary Damper Verification

To investigate the behavior of the stacked honeycombs inside the primary strut during compression, the strut is positioned vertically under the drop mass of the drop tower in a way that the drop mass can only cause axial loads. Some of the tests in this series are performed with a Plexiglas tube as main tube of the primary strut to allow the visual observations (see Fig. 18).

Fig. 18: Primary shock absorber before and after test

The honeycomb crash absorbers are cut into cylinders and are separated by sliding rings from each other. Three absorbers with different densities are stacked above each other in this manner. The foot pad is replaced by a cylindrical steel block. During the test the drop weight hits the block which is connected to the inner tube of the main strut. The inner tube compresses the honeycomb absorbers which are sitting on the ending cap of the leg. The cap is connected by a joint to the bottom plate. A 3D-force sensor is embedded above the joint measuring the forces on this side of the setup. Acceleration sensors measure the accelerations on the drop weight side. A laser measures the position of the inner tube relatively to the outer tube. Fig. 19 shows the force-time curves of five experiments emphasizing the very good repeatability in the behavior of dampers.

The three load plateaus on the left side represent the crushing of the single stages. The repeated force peaks in the middle part of the diagram represent the spring-backs of the drop mass, which do not compress the third honeycomb stage any further.

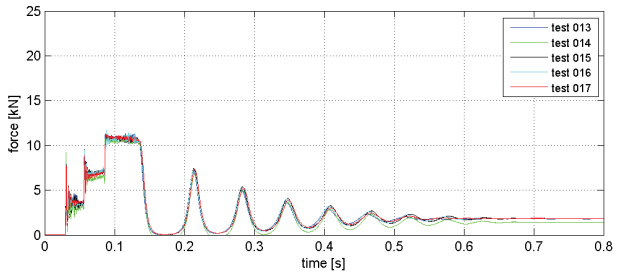

Fig. 19: Typical force history of a series of test

The stroke-time and force-stroke curves for the same experiments are summarized in Fig. 20 and Fig. 21.

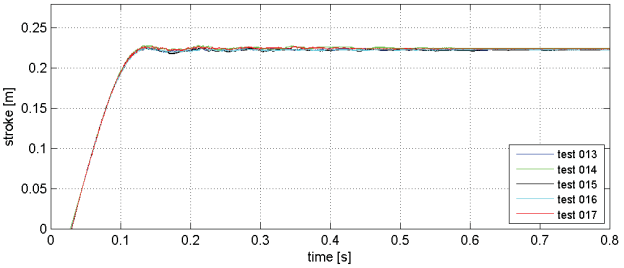

Fig. 20: Typical stroke history of a series of test

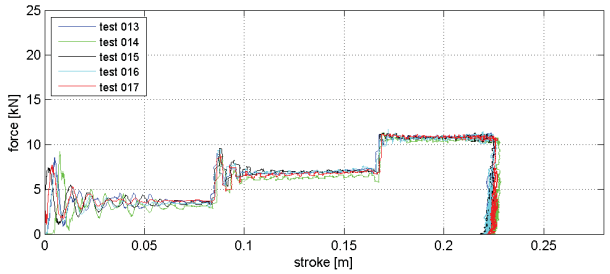

Fig. 21: Typical main damper force-stroke characteristics

The performed experiments demonstrate clearly that the honeycomb dampers can efficiently and reliably limit the loads during a landing like event.

3.4. Single Leg Drop Tests

Finally drop tests with a complete landing leg are performed. Both in Chapter 1.2 presented leg designs (Cantilever Leg and Inverted Tripod) are investigated.

3.4.1. Test Matrix

The setup is designed in a way that the orientation of the primary strut regarding the bottom plane can be changed. The setup can be tilted and rotated at the same time, so a variety of possible landing scenarios can be investigated. See Fig. 22 for the test matrix. The listed tests including the footpad sensor will be performed at the end of 2011 for the verification of the sensor itself.

In both configurations, the leg is connected to the test setup at three points. A universal joint is constraining the ending cap of the main tube of the main strut. The secondary struts are connected to the setup with bending rods.

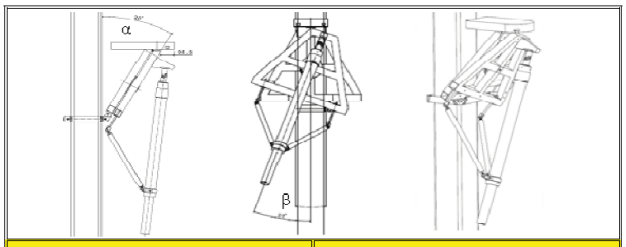

Cantilever Leg (15 Drops)				
β [°] \ α [°]	0	10	20	30
0	3	1	1	1
10	1	1	3	1
20	1	1	1	

Inverted Tripod Leg (15 Drops)				
β [°] \ α [°]	0	10	20	30
0	3	1	1	1
10	1	1	3	1
20	1	1	1	

Leg on mix. Terrain (10 (12) Drops)				
β [°] \ α [°]	0	10	20	30
0	1+1+1 C 1+1+1 IT	0	0	0
10	0	0	1+1+1 C 1+1+1 IT	0
20	0	0	0	

Breadboard + FP Sensor on mix. Terrain (20 Drops)				
β [°] \ α [°]	0	10	20	30
0	tbd	tbd	tbd	tbd
10	tbd	tbd	tbd	tbd
20	tbd	tbd	tbd	

Fig. 22: Test matrix of leg drop tests

Forces are measured at the ending cap and at the joint between the foot pad and the inner tube of the main strut with 3-D force sensors (MP01-03 and MP04-06 respectively). Also 1-D force sensors (MP07 and MP08) measure the axial loads in both secondary struts. The movements of the joints between the bending rods and the secondary struts are measured with three draw wire sensors at each joint (MP09-11 and MP12-14). The three sensors at each joint are positioned perpendicular to each other allowing measuring the exact position of the joint in 3D. The relative displacement of the inner and the outer tube of the main strut is measured with a laser (MP15). Furthermore, the linear acceleration of the drop mass is measured (MP16).

The leg falls into a box filled with sand to represent lunar or martian soil. For the representation of hard ground contact, the sand has been compacted and covered by a wooden panel or/and an oiled thin steel sheet representing different ground friction scenarios. In some special cases the free sliding of the foot pad was stopped directly at the point of contact using wooden blocks during the experiments (see lower-left part of Fig. 23).

3.4.2. Cantilever Leg Configuration

Some of the results acquired with the Cantilever Leg configuration are shown in Fig. 24 to Fig. 26. All the presented results are shown for the rotated leg (β=10°, α=20) representing an oblique landing scenario at 4m/s impact velocity.

The skewed landing shock is especially good visible in the secondary struts force diagrams. The left strut is compressed (MP08) and the right (MP07) is loaded in tension. Again the loads in secondary and primary struts are reproducible. The unfiltered acceleration peaks (MP16) are remarkably low for all tests (<10g). The loads at the ending cap (MP03) are larger than at the foot pad (MP06), because of the added lateral forces from the secondary struts.

Fig. 23: Test setup of Cantilever Leg drop test

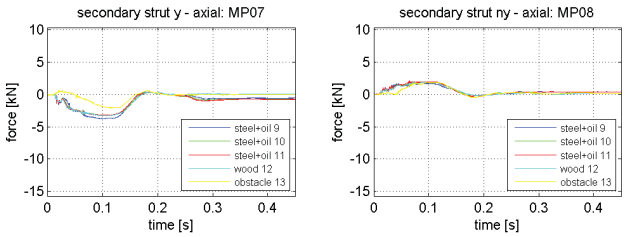

Fig. 24: Secondary struts force histories Cantilever Leg Drop tests

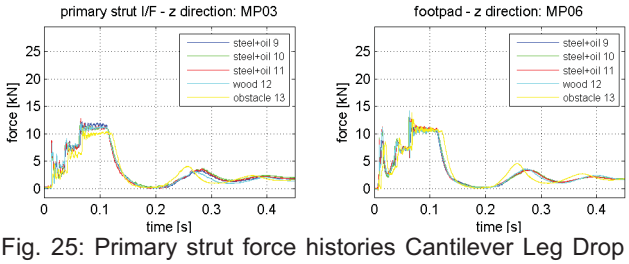

Fig. 25: Primary strut force histories Cantilever Leg Drop tests

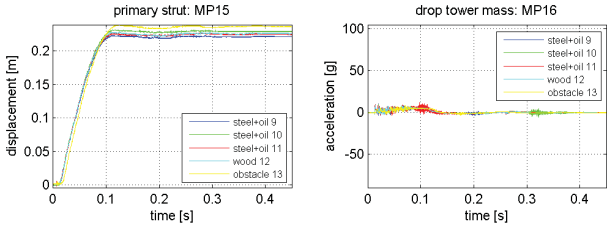

Fig. 26: Primary damper stroke history and drop tower mass acceleration of Cantilever Leg Drop tests

When the footpad is constrained by an obstacle, in this particular load case more energy is absorbed by the honeycomb dampers, which is visible in the large relative displacement (MP15) of the inner tube (= larger compression length). Also the axial force at the ending cap (MP03) is smaller due to lower lateral forces (MP07+MP08). The aim here was to simulate an obstacle (for example a stone) in the landing area. The influence of the different types of ground friction, simulated by the wooden plate and the oiled steel plate seem to be negligible on the first view. Due to the curved shape of the

pad most probably no clear oil film was established. Thus, the friction was higher than intended.

3.4.3. Inverted Tripod Configuration

In Fig. 28 to Fig. 30 the results for the same testing conditions as presented for the Cantilever Leg configuration are shown for the Inverted Tripod configuration. The most obvious difference between the two configurations is the much lower ground clearance and the much longer sliding bath of the footpad for the Inverted Tripod (see Fig. 27).

Fig. 27: Test setup of Inverted Tripod leg drop test

Despite the same kinetic energy, only two of the three honeycomb dampers are compressed (see the force steps in MP03 and MP04), because more energy is dissipated by the bending rods. On both sides, the secondary struts are compressed shortly after the impact bending the rods in one direction – then the forces reverse bending the rods back (MP07 and MP08). This force reversal can also be seen in the relative displacement of the inner tube (MP15). On the contrary to the Cantilever Leg the forces at the foot pad (MP06) are at the beginning significantly larger than at the ending cap (MP03) since the secondary struts are attached to the inner tube close to the footpad. After the force reversal in the secondary struts, the force at the footpad drops.

Also in this configuration the “obstacle”-case influence the behavior of the system significantly. Even more energy is absorbed by the bending rods, especially on the left side (see the forces in the secondary struts, MP07 and MP08). Due to limited kinematics, no force reversal occurs in this case. The high axial force in the left secondary strut (MP08) leads to higher forces at the foot pad. After the kinetic energy is absorbed the energy stored in the elastic deformation of the bending rods pushes the leg up (see MP15).

The source for the "strange" behavior of the displacement signals at MP15 is an excessive penetration of the sand by the footpad. At the end of the test, the pad was completely covered by sand and the laser was not able to point at the reflection plate anymore.

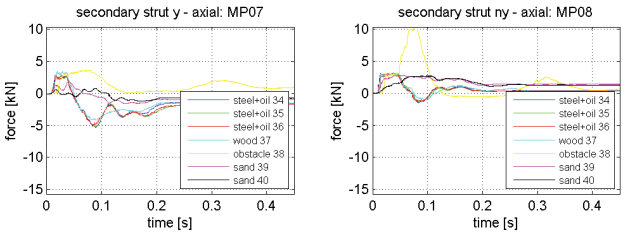

Fig. 28: Secondary struts force histories of Inverted Tripod Leg Drop tests

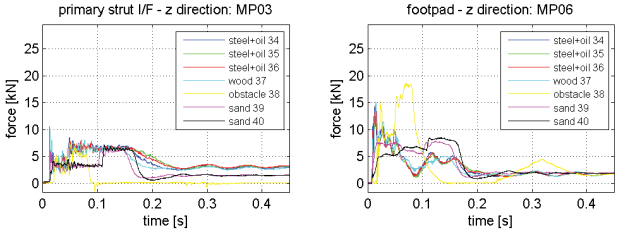

Fig. 29: Primary strut force histories of Inverted Tripod Leg Drop tests

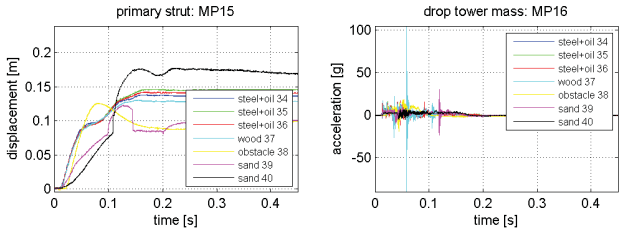

Fig. 30: Primary damper stroke history and drop tower mass acceleration of Inverted Tripod Leg Drop tests

4. SUMMARY AND CONCLUSIONS

Based on former successful missions to Moon and Mars and on future mission scenarios like the European Lunar Lander and the ESA Mars Precision Lander, two generic landing leg breadboards and representative test requirements have been defined and manufactured.

The critical elements and the key functionalities of the two breadboards (Inverted Tripod and Cantilever Leg Configuration) have been identified and a bottom - up test and a verification approach has successfully been applied to demonstrate technological readiness up to TRL 5. Both breadboards showed excellent performance under all experimental conditions and on all level of system integration, demonstrating the high efficiency and reproducibility of the chosen design.

One drawback with a minor influence on the design came up after the investigation of the temperature influence on the damper performance. Being exposed to higher temperatures (in the test up to 140° C), the damper performance loss reaches unacceptable values of up to -30% compared to nominal conditions. This demonstrated clearly the need for extensive thermal protection for the damping elements, as already observed within the NASA Apollo programme [RD1].

5. REFERENCES

[RD1] W. F. Rogers, Apollo Experience Report - Lunar Module Landing Gear Subsystem, NASA TN D-6850, June 1972